Integrity Testcase Experimentation Results Within GSTB-V1

Wolfgang Werner, Ingrid Deuster
IfEN Gesellschaft für Satellitennavigation mbH (IfEN GmbH), D-85586 Poing, Germany

Francisco Amarillo Fernandez
European Space Agency (ESA), Noordwijk, The Netherlands

BIOGRAPHIES

Wolfgang Werner received a diploma in Computer Science from the University of Technology in Munich in 1994. He worked as a research associate at the Institute of Geodesy and Navigation (IfEN) in the field of high-precision differential GPS (DGPS), ambiguity resolution and airport pseudolite (APL) research. In 2000 he received his Ph. D. from the University FAF Munich. Since 1999 he is Technical Director of IfEN GmbH. Having been responsible for the EGNOS Independent Check Set algorithm development, he is currently working on Galileo integrity algorithms.

Ingrid Deuster holds a diploma in Geodesy from the University of Stuttgart. In 1998/1999 she worked as a research associate at the Institute of Photogrammetry and Cartography of the University FAF Munich. She joined IfEN in 1999 as a systems engineer and has worked since then in the field of satellite navigation integrity. She was involved in the EGNOS Check Set algorithm development and in the Galileo Integrity Performance Assessment (GIPA) early trials. Currently she is working for the GSTB-V1 project.

F. Amarillo-Fernandez is Satellite Navigation Engineer in the TEC-ETT section of the European Space Agency supporting the coordination of GSTB-V1 experimentation activities for the Galileo Project Office in Noordwijk (The Netherlands). He received his Master's Degree in Telecommunication and Surveying Engineering by the Polytechnic University of Madrid, Spain in 1997 and became Specialist in Satellite Communications, by the same University in 2001. He collaborates actively in the consolidation of the Ground and User Segment Algorithms for Integrity Monitoring, Orbit Determination and Time Synchronisation.

ABSTRACT

Within the European Galileo Satellite Test Bed (GSTB-V1) experiments are conducted with the goal of assessing Galileo integrity performance and consolidating integrity architecture. For this reason an experimental integrity processing facility (E-IPF) has been developed and put into place within the GSTB-V1 processing centre (GPC). The routine operation of the system has begun in the first half of this year and the system is now generating a set of daily and long-term core products based on real GPS data but with Galileo navigation and integrity algorithms.

First experiments cover mainly the pre-processing and the integrity system budget allocation. Within the first experimentations the performance of the complete pre-processing chain is analysed in terms of total range and synchronisation error. It turns out that for the purpose of integrity processing the pre-processing of raw measurements is a critical trade-off between few high-accuracy or many low-accuracy measurements that will be a major contributor to overall integrity performance. The signal-in-space monitoring accuracy (SISMA) has been analysed.

The signal in space error (SISE) is an (instantaneous) value composed of the components orbit and clock error, which needs to be estimated as accurate as possible by the E-IPF. Valid SISE estimation candidate algorithms for the Galileo integrity system are a tangential plane estimation algorithm as well as a (robust or non-robust) direct error component estimation algorithm at the satellite coming from earlier phases of the Galileo project.

This paper presents the current status of the integrity experimentation and provides the first results obtained so far in the pre-processing and SISMA performance areas based on the GSTB-V1 sensor station network.

EXPERIMENTAL IPF

The facility that has been developed for performing the integrity experimentation is the Experimental Integrity Processing Facility (E-IPF). Its processing kernel has integrated a set of more than 240 algorithmic modules that perform all required processing tasks. All the available modules can be inserted in a configuration and linked together as needed. This means that not only the algorithm parameters can be set, but the complete processing chain can be configured in some kind of graphical programming allowing the high flexibility needed for the experimentations in the integrity testcase.

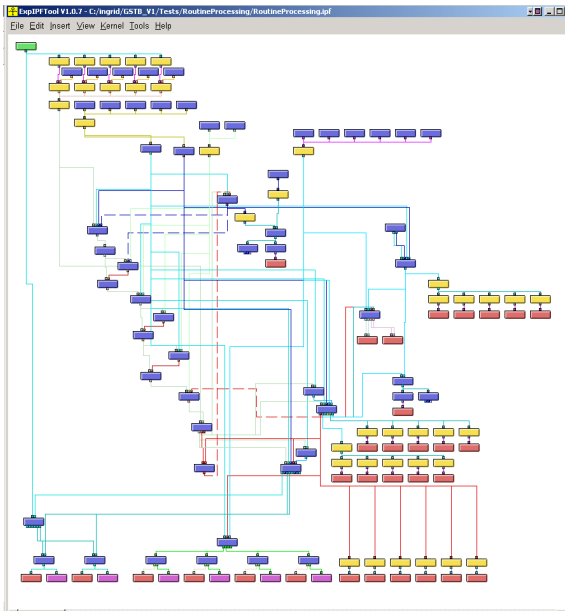

Figure 1: Typical E-IPF configuration

The details of the E-IPF design have already been described in some other papers and are not repeated here (see *Werner et al., 2003*, *Werner et al., 2004*).

COMMISSIONING PHASE RESULTS

In an initial commissioning phase, three different scenarios have been processed and analysed within the GSTB-V1 integrity experimentation:

- GPS only
- GPS augmented by Galileo algorithms
- Galileo simulation

The first two scenarios are based on real data processing of day 49 in 2004. The data that have been used are taken from 26 IGS stations that are used within the GSTB-V1. The third scenario is a pure simulation, but based on comparable environmental assumptions.

The processing chain is identical for both scenarios working on real measurements. In the simulated scenario ionosphere and troposphere are not modelled and therefore the algorithms to remove these corrections are excluded. Key parameters of the processing chain are:

- Elevation angle of 12.5°
- Hatch filter constant 180 s
- Clock estimation with filter constant of 60 s and FDI capability
- Ionospheric free linear combination in case of real data
- Tropospheric correction based on ESA Blind model in case of real data (see *ESA, 2003*)
- Protection levels are computed according to MOPS (see *RTCA, 1999*)
- Horizontal and vertical alarm limit are set to 12 m and 20 m respectively.
- UERE for availability maps is elevation dependent and depictured in figure 2 (Avail, green line)

For Stanford plots (see *Stanford University, 1999*) different UERE budgets as shown in figure 2 have been used. For the GPS only scenario a UERE budget according to MOPS Class 3/4 receiver equipment was chosen from 0.40 m at 90° to 0.83 m at 10° (blue line). For the GPS augmented scenario the UERE is set to 0.85 m (magenta line), which is more conservative in comparison to GPS only. For Galileo simulation the UERE starts with 0.25 m at 90° to 0.45 m at 10°(red line).

Based on the same sensor station network the Galileo simulation was set up with a nominal Walker constellation (3 planes, 9 satellites per plane, an inclination of 56° and a circular radius for orbit of 29993707.0 m). Orbit errors in radial, long-track and cross-track of 0.4 m, 1.2 m and 0.8 m respectively were introduced. Clocks are simulated with bias (2e-4 sec), drift (1e-10 sec/sec) and Gaussian noise of 1.5e-9 sec (= 0.45 m). The SISA for all satellites was set to 0.8 m.

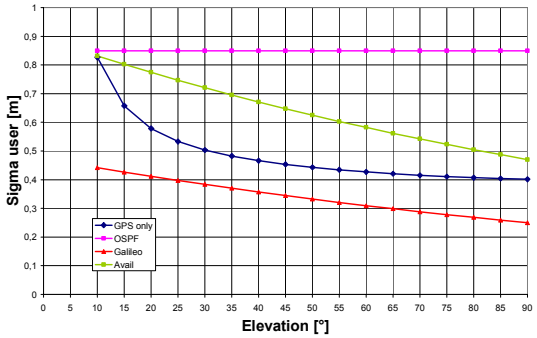

Figure 2: UERE budget for all scenarios

All of the results have been obtained by the E-IPF SW. In this paper we present the availability and Stanford plots, as these are the most important core products for analysing the end-to-end system integrity performance. Both, vertical and horizontal types of plots are given with alarm limits of 12 m (horizontal) and 20 m (vertical).

GPS Only Processing

In this scenario, GPS real data are processed together with of the GPS broadcast navigation messages. Figures 3 and 4 show the availability of GPS only. Only a protection level computation has been performed, no integrity processing is included, i.e. no integrity algorithm is included. When integrity algorithms are included, the results become even worse due to "not monitored" or "don't use" flagged satellites. The assumed value for the SISA was set to 2 m, which correlates to the URA values as broadcast in the GPS navigation messages of this day. As can be seen from the availability plots, horizontal availability for 12 m is around 60% and vertical availability for 20 m it is less than 50%.

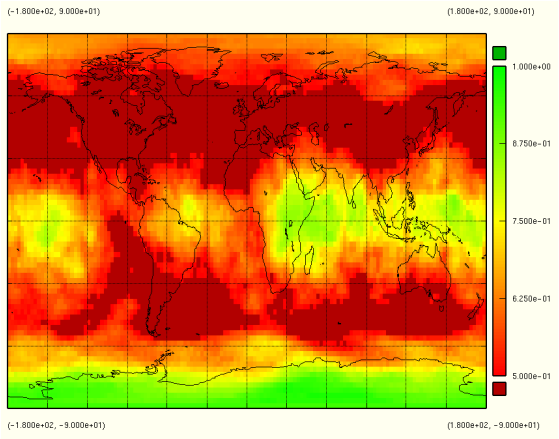

Figure 3: GPS only: Availability (horizontal, HAL 12 m)

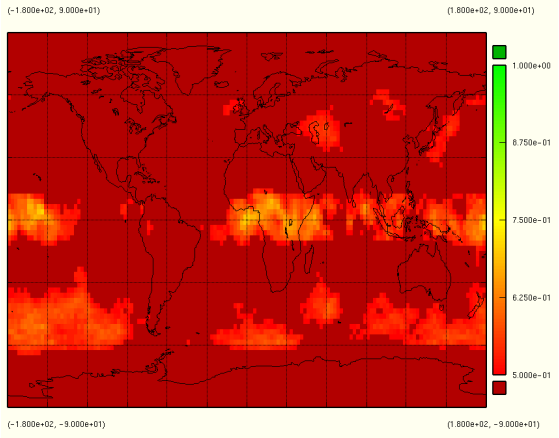

Figure 4: GPS only: Availability (vertical, VAL 20 m)

Figures 5 and 6 show the resulting Stanford plots. In this case the processing chain includes integrity algorithms providing integrity information, which is considered by the user. It is assumed that the SISA is equal to the URA for integrity purposes.
The Stanford plots reflect results of the availability for certain user positions, here the sensor station positions. It is obvious that the frequency peaks are concentrated near the alarm limit and even above, and therefore the non-availability rate is quite high. The spreading of the samples indicates a fitting UERE budget with no further margin for improvements.

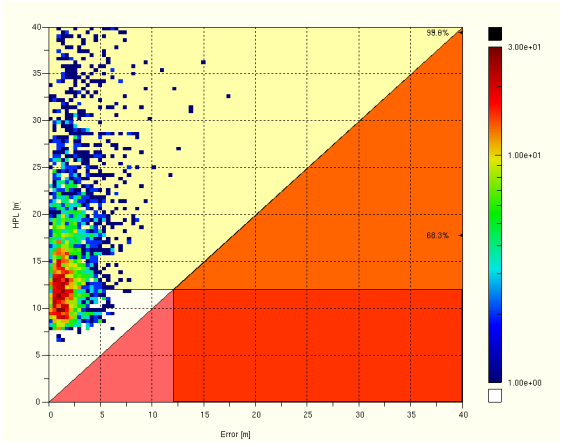

Figure 5: GPS only: Stanford Plot (horizontal, HAL 12 m)

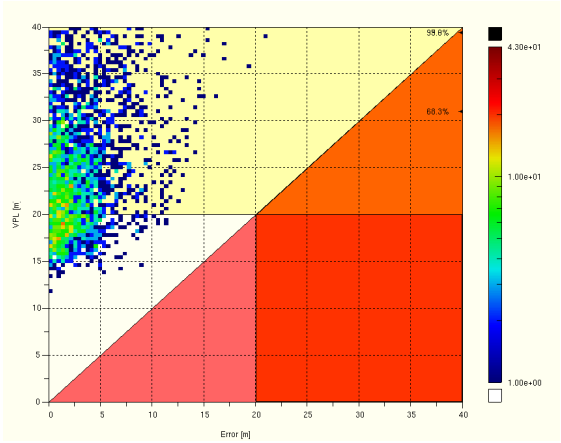

Figure 6: GPS only: Stanford Plot (vertical, VAL 20 m)

GPS Processing Augmented by Galileo Algorithms

This scenario is the standard GSTB-V1 scenario: GPS real data are processed but making use of Galileo OD&TS (orbit determination and time synchronisation) algorithms. This means the same raw data than in the first scenario have been processed but with the navigation messages as provided by the E-OSPF. Furthermore, a standard E-IPF integrity processing was included.
The availability and Stanford results are shown in the four figures 7 to 10. In comparison to the GPS only case the frequency peaks are clearly below the alarm limits. In addition, the shape of the distributions (elongated in y-axis direction) shows the conservative assumption of the elevation-independent UERE of 0.85 m. This means there is still some margin for the UERE budget.

The results with Galileo algorithms provide a much better performance than GPS only, which is due to the accuracy of the E-OSPF navigation message based on the ground sensor station (GSS) network.

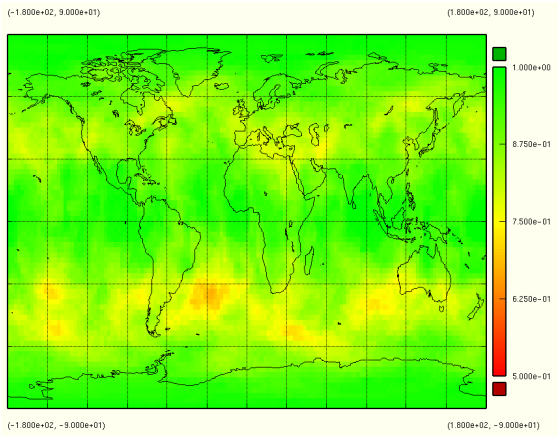

Figure 7: GPS augmented: Availability (horizontal, HAL 12 m)

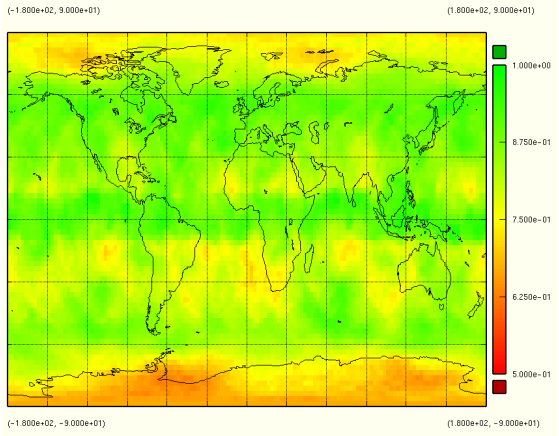

Figure 8: GPS augmented: Availability (vertical, VAL 20 m)

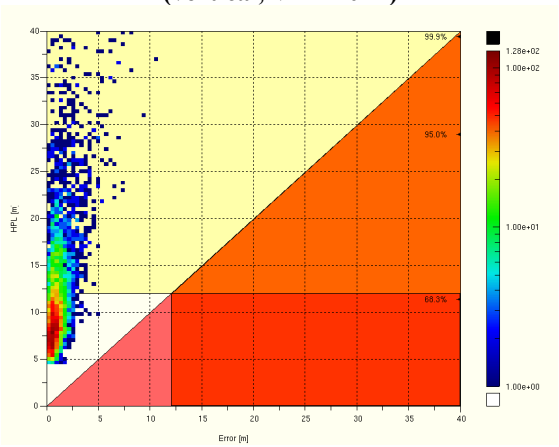

Figure 9: GPS augmented: Stanford Plot (horizontal, HAL 12 m)

What is interesting to see in the results is, that the availability map is a combined result of the GPS satellite constellation and the GSTB-V1 sensor stations network.

A similar structure can be seen in the availability maps of both, the GPS augmented case and the GPS only case. GPS simulations frequently show six wandering integrity "holes" - three in the northern hemisphere and three in the southern hemisphere. Tracks of these can e.g. be seen in the two red horizontal areas in figure 3, and the slightly degraded yellowish areas in figure 7. The results here are accumulated over 24 hours and so show horizontal stripes.

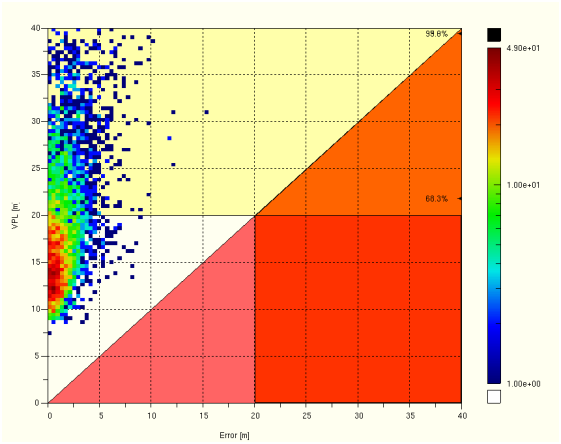

Figure 10: GPS augmented: Stanford Plot (vertical, VAL 20 m)

Considering the sensor station network, a bad monitoring coverage was identified over the southern Atlantic. This was due to unavailability of monitoring data in this area. So, in figure 10, the degradation due to integrity monitoring can also be seen on top of the GPS constellation structure.

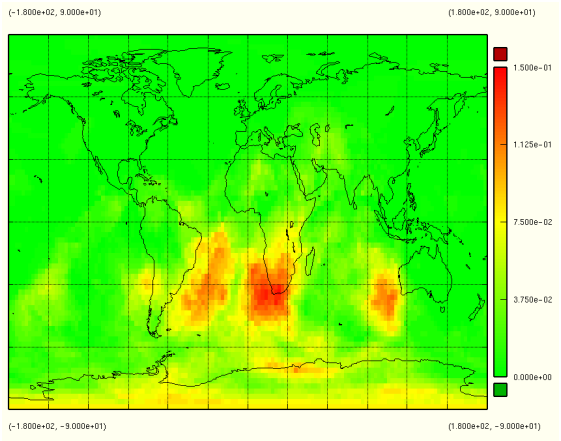

Figure 11: GPS augmented: degradation of availability due to integrity monitoring (vertical, VAL 20 m)

The degradation of availability due to integrity monitoring is strongly dependent on the sensor station network and the vertical example is depicted in figure 11. This degradation shows the difference between navigation availability only (no integrity processing included) and availability of integrity

("not monitored" or "don't use" satellites removed from the protection level computation). The monitoring weakness over South Africa due to the GSS network is evident from this figure.

Galileo Simulation

A simulation has been performed for the Galileo scenario. In this scenario the standard Galileo constellation (Walker 27/3/1, orbit radius 29993.707 km and 56.0° inclination) has been used as a baseline. The same GSS network was used as in the other cases above. The duration of the simulation was also set identical to 24 hours as in the other cases.

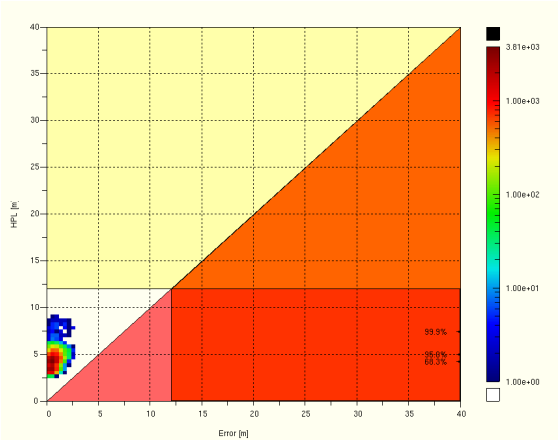

Figure 12: Galileo Simulation: Stanford Plot (horizontal, HAL 12 m)

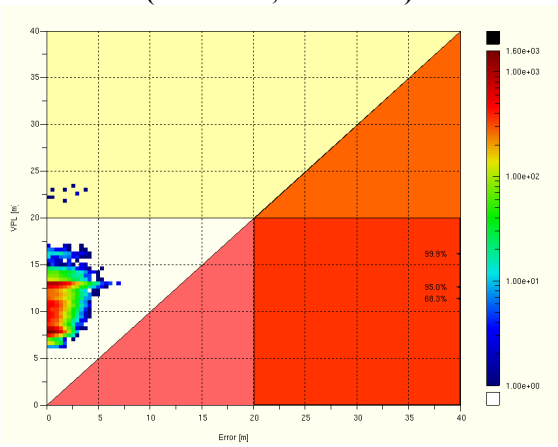

Figure 13: Galileo Simulation: Stanford Plot (vertical, VAL 20 m)

The availability plots for the Galileo simulation are all green and therefore not depicted here. An overall availability of 99.5 % has been obtained, what matches the current Galileo requirement.

INTEGRITY EXPERIMENTATION

The first part of the integrity experimentations was mainly dedicated to pre-processing characterisation in terms of range accuracy and synchronisation performances. Together with the satellite constellation and monitoring stations network, the quality of the pre-processed data is one of the main drivers for the overall integrity check performance. Hence, to understand the achievable pre-processing performance it is necessary to analyse in detail the quality of the input data on the one hand and to evaluate the propagation through the pre-processing on the other hand. Difficult trade-offs can then be performed between a high number of low-quality measurements and a lower number of high-quality measurements. This trade-off is e.g. relevant for pre-processing tuning parameters like elevation masking angles or smoothing time constants. To investigate the performance of the pre-processing, the first step is to analyse the quality of the input data. For this reason, the input data has been analysed in terms of cycle-slip occurrence and code noise.

Cycle Sip Detection

During experimentation it turned out, that some of the sensor station clocks showed a short-term instability, which violated the assumption of a free-running clock in the integrity monitoring stations. The cycle slip detection algorithm is based on a 3rd-order time-difference indicator of carrier phase measurements. This indicator is compared with a threshold to decide, if a cycle slip is present or not. Figure 14 shows an example where the observed characteristic for the 3rd-order time-difference is identical for all satellites tracked by this station. This proves that the problem has a common source and is related to the short-term stability of the station clock. From this figure it is also visible, that the 3rd-order time-difference indicator at epoch 20, 35 and 50 is clearly above the threshold of ½ cycle L1P (Thd L1P, pink lines). As a consequence of this the false detection rate was quite high for some of the stations.

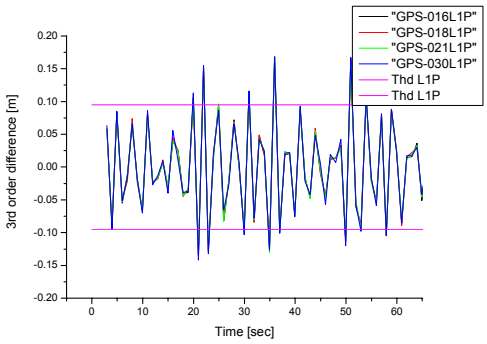

Figure 14: 3rd-order time-difference on phase measurements to one station

A new algorithm has therefore been developed to take into account such ill effects. The main idea of this new algorithm is to compute a mean value of

the 3rd-order time-difference indicator ($\overline{\Delta^3}$) for each station (i) and remove this mean value from each line of sight (LOS) 3rd-order time-difference-indicator to this station ($\Delta^3_{cor,i}$). To protect the mean value from outliers an additional FDI algorithm is used.

$$\Delta^3(t) = \Phi(t) - 3\cdot\Phi(t-1) + 3\cdot\Phi(t-2) - \Phi(t-3)$$

$$\overline{\Delta^3}(t) = \frac{1}{N}\sum_{i=1}^{N}\Delta^3_i(t) \quad \text{(where i loops across LOS)}$$

$$\Delta^3_{cor,i}(t) = \Delta^3_i(t) - \overline{\Delta^3}(t) \quad \text{(where i is LOS index)}$$

To ease readability most indices have been omitted in the above equations.
In figure 15 the original 3rd-order time-difference-indicator (black) and the 'corrected by mean' 3rd-order-indicator (red) are depicted for GPS-16 L1. At epoch ~3000 a clear peak in the red line is visible, which indicates a real cycle slip. So with this kind of algorithm small cycle slips can be separated from clock characteristics and therefore they are detectable.
In table 1 the number of detected cycle slips, based on the new algorithm is given for the complete network of 25 stations as well as the best and the worst station, THTI and FAIR respectively. The detection algorithm was configured to detect and repair cycle slips with a minimum magnitude of one cycle.

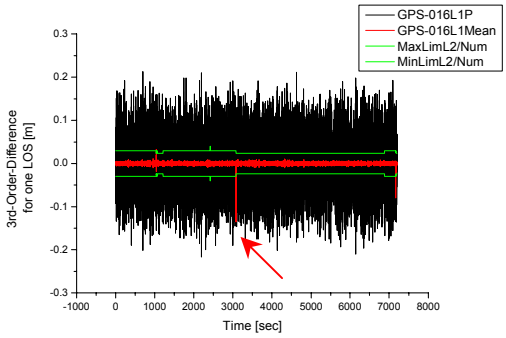

Figure 15: 3rd order difference indicators for one LOS and corrected by mean

	Number of cycle slips			Cycle slip rate
	L1P	L2P	L1P + L2P	[cycle slip / 30 s]
Total	11313	9159	20472	3.3e-3
THTI	0	0	0	0.0
FAIR	1936	1991	3927	1.4e-2

Table 1: Cycle-slip occurrence

For the experimentation a cycle slip rate of one cycle per 30 seconds and LOS is considered as feared event. Therefore the mean cycle slip rate of ca. 3.3e-3 cycle slips per 30 seconds is in the expected range for normal processing conditions.

Code noise

Figure 16 and 17 show time-differenced code-minus-carrier (CmC) statistic for all stations accumulated over one week of data. To obtain code noise the CmC value has to be divided by $\sqrt{2}$.

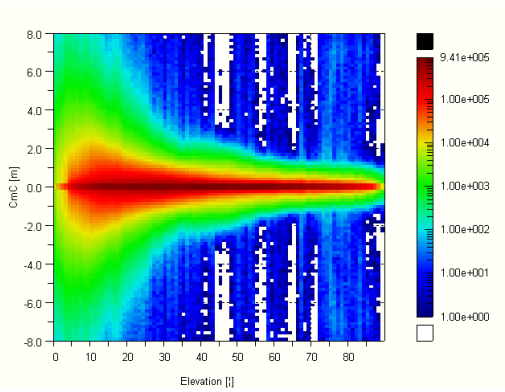

Figure 16: Time differenced code-minus-carrier vs. Elevation (all Stations)

The elevation dependent CmC root-mean-square characteristic (figure 17) shows more or less expected behaviour up to an elevation angle of 70°. Above this elevation angle the CmC value increases again. This phenomena is linked to L2P measurements of a couple of stations, which are equipped with an identical receiver type working in some special mode. Further analysis is ongoing on this issue.

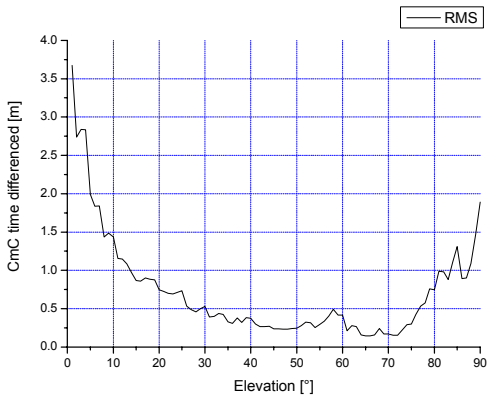

Figure 17: Time differenced code-minus-carrier vs. Elevation (RMS)

The characteristic of CmC for the complete network is in the expected range for GPS measurements. Nevertheless the network behind these results is very inhomogeneous. In the figures 18 to 23, the time-differenced code-minus-carrier statistics for a few examples of individual stations are shown. It can be seen, how differently the station code noise characteristics can be.

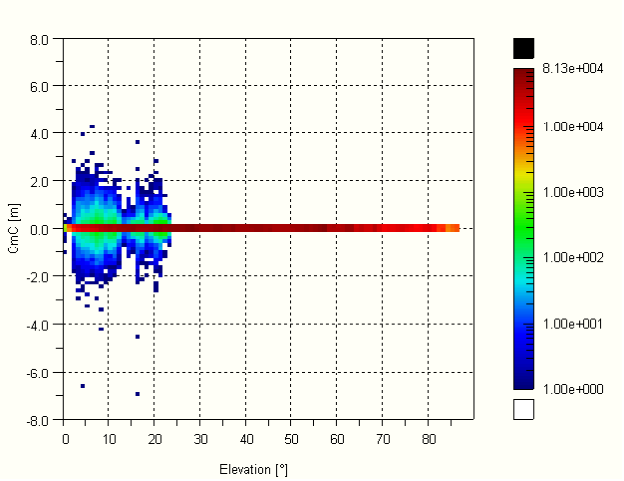

Figure 18: Time differenced code-minus-carrier vs. Elevation (Station #04)

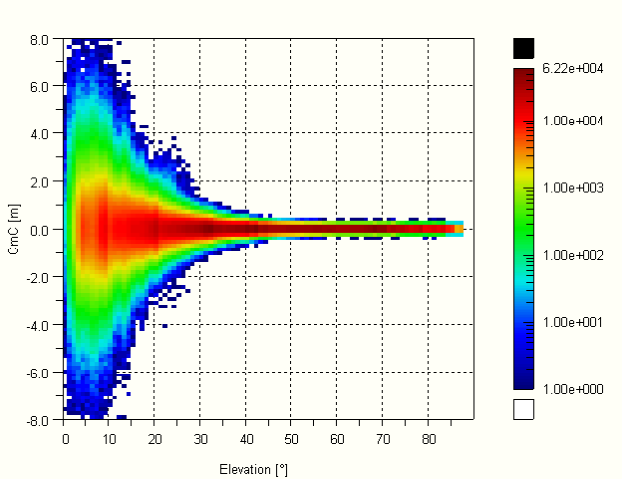

Figure 19: Time differenced code-minus-carrier vs. Elevation (Station #08)

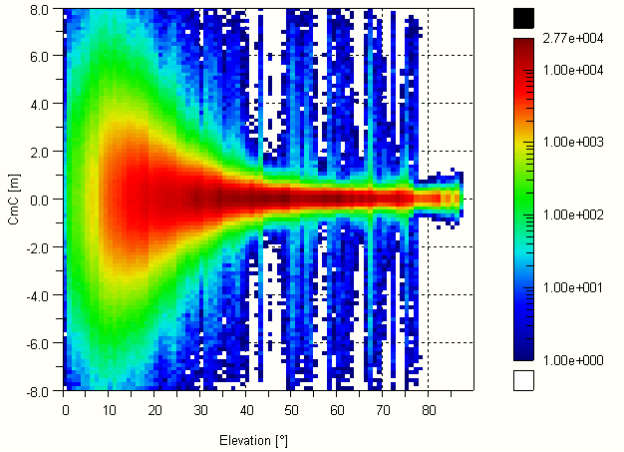

Figure 20: Time differenced code-minus-carrier vs. Elevation (Station #15)

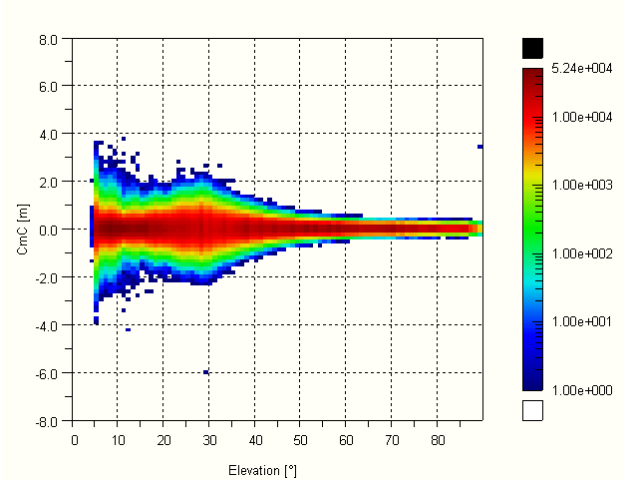

Figure 21: Time differenced code-minus-carrier vs. Elevation (Station #19)

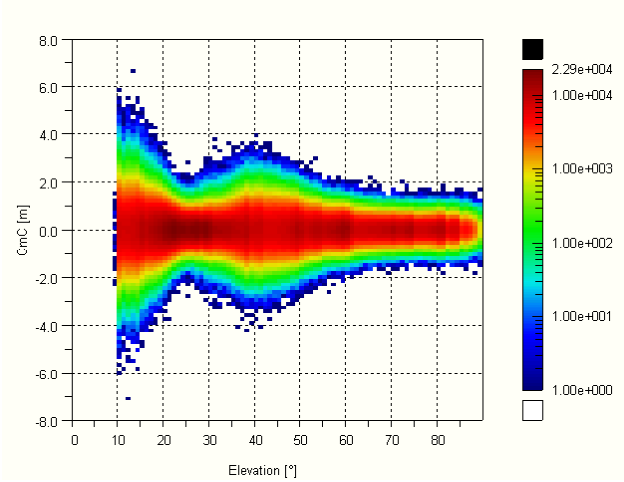

Figure 22: Time differenced code-minus-carrier vs. Elevation (Station #21)

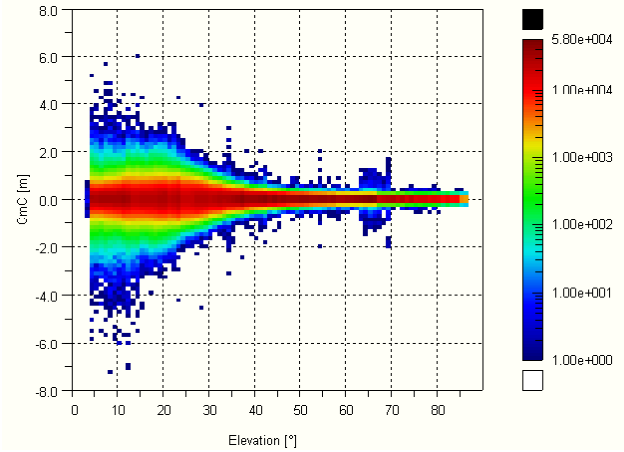

Figure 23: Time differenced code-minus-carrier vs. Elevation (Station #24)

Pre-processing Performance

The pre-processing performance was analysed in terms of range accuracy and synchronisation error statistics. IGS data (sensor station and satellite clocks as well as satellite orbits in RINEX clock and SP3 file format) have been used as a reference. The accuracy of IGS data is not taken into account, and thus, contribute to the integrity algorithm error budget. Due to the very different characteristics of individual stations, four sub-sets of stations have been defined as shown in table 2, where reference data was available.

Range accuracy before synchronisation

The range accuracy before synchronisation is mainly driven by the capability to detect and repair cycle slips and the smoothing time constant of the Hatch filter. With a filter time constant of 600 seconds and a cycle slip detection threshold of ½ cycle the most promising results have been obtained. With these configuration parameters of the pre-processing enough observations remain for the clock synchronisation as well as for the SISE estimation algorithm. Of course, these parameters are linked to the sensor station network and may be changed for other networks.

Station Name	Id	Subset #1	Subset #2	Subset #3	Subset #4
BAN2	15	x			
FAIR	25	x	x	x	x
GLPS	22	x	x	x	x
GOLD	24	x	x	x	
KERG	21	x	x	x	x
KIRU	5	x	x		
KOUR	1	x	x	x	x
MAS1	3	x	x	x	x
MIZU	8	x	x	x	x
MKEA	23	x	x	x	
NNOR	4	x	x	x	x
PERT	29	x	x	x	x
RIOG	19	x	x		
THTI	20	x	x	x	
TIDB	26	x	x	x	x
VILL	6	x	x	x	x

Table 2: Definition of Station Subsets

In figure 24 the accumulated range accuracy before synchronisation based on one week of data is depicted. The contamination of the result by the inhomogeneous station network can be seen clearly. Removal of the stations KIRU and RIOG improves the budget significantly (see green and blue curves). By removing these two stations the overall range accuracy improves by 0.185 m from 0.548 m to 0.363 m. In table 3 the obtained elevation independent range accuracy before synchronisation for all subsets is listed.

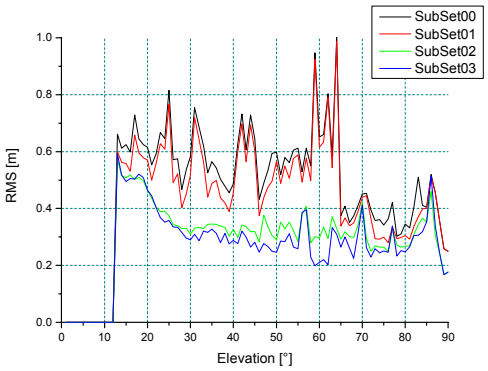

Figure 24: Range Accuracy Before Synchronisation, all Station Sub-Sets

	Mean [m]	StdDev [m]	RMS [m]
Subset #1	0.079	0.589	0.594
Subset #2	0.082	0.542	0.548
Subset #3	0.067	0.357	0.363
Subset #4	0.070	0.333	0.341

Table 3: Range Accuracy Before Synchronisation

Synchronisation Error

The synchronisation algorithm used for the experimentation is a direct synchronisation combined with a filter. The result of the trade-off with different filter time constant is presented here. In figure 25 and 26 the synchronisation errors in seconds for different filter time constants T of 60 sec and 5 sec for the clock filter are depicted. All other parameters of the pre-processing are identical (cycle slip detection threshold 3 cycles and smoothing time constant of 180 sec). For this kind of trade off one day of data was selected.

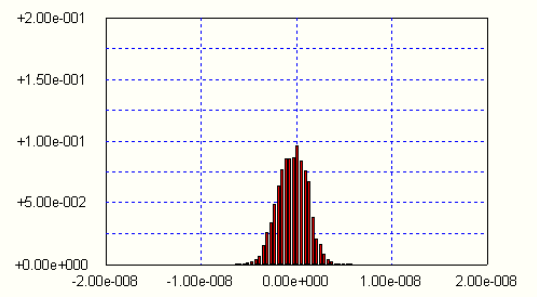

Figure 25: Synchronization Error [sec] (T = 60 sec)

As can be seen in the histograms of figure 25 and 26 the synchronisation error increases by reducing the filter time constant from 60 sec to 5 sec. The top of the histogram is higher and the density curve is thinner for 5 sec. The figure 27 was obtained with a Hatch filter time constant of 600 sec, a cycle slip

detection threshold of ½ cycle and a clock filter time constant of 5 sec accumulated over one week of data.

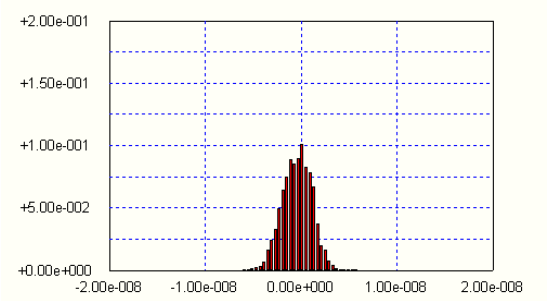

Figure 26: Synchronization Error [sec] (T = 5 sec)

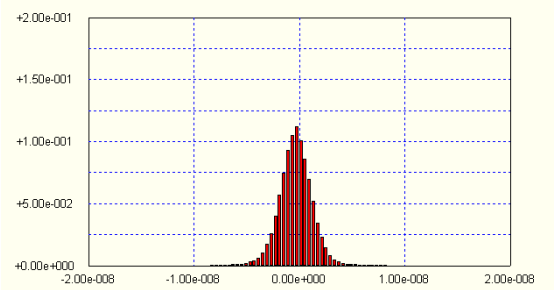

Figure 27: Synchronization Error [sec] (T = 5 sec)

	Mean [m]	StdDev [m]	RMS [m]
Total	-0.079	0.756	0.760
STA-001	0.056	0.467	0.470
STA-003	0.044	0.343	0.346
STA-004	-0.265	0.702	0.751
STA-005	0.030	1.359	1.359
STA-006	0.130	0.295	0.323
STA-008	0.006	0.415	0.415
STA-015	0.251	2.121	2.135
STA-019	-0.326	0.581	0.666
STA-020	-0.193	0.418	0.461
STA-021	-0.288	0.337	0.443
STA-022	-0.248	0.437	0.502
STA-023	0.017	0.535	0.536
STA-024	0.011	0.587	0.587
STA-025	0.042	0.286	0.289
STA-026	0.003	0.407	0.407
STA-029	-0.195	0.453	0.494

Table 4: Synchronisation Error for Individual Stations

The data set behind the histogram above is given in table 4. As can be seen in the histogram the synchronisation error is not exactly centred, which is also reflected in the total mean value of -0.08 m. The mean synchronisation error is 0.76 m with a range form 0.289 m up to 2.135 m.

The direct synchronisation algorithm is a bias estimation and therefore absorbs common remaining biases (e.g. remaining tropospheric effects, etc.) on all LOS to one station into the clock. After applying the estimated clock to the ranges the offset nearly vanished as listed in table 5. The range accuracy after synchronisation is given table 5 and depicted in figure 28 for the different sensor station subsets. In figure 29 the range accuracy for some single station is shown.

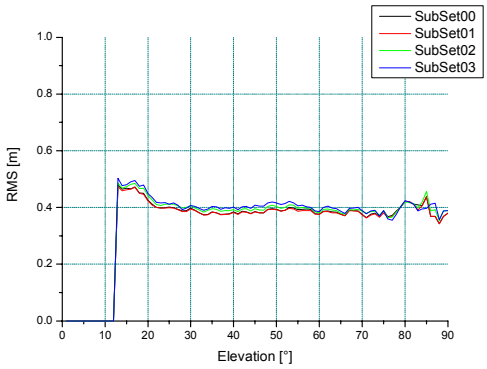

Figure 28: Range Accuracy after Synchronization (RMS), all Station Sub-Sets

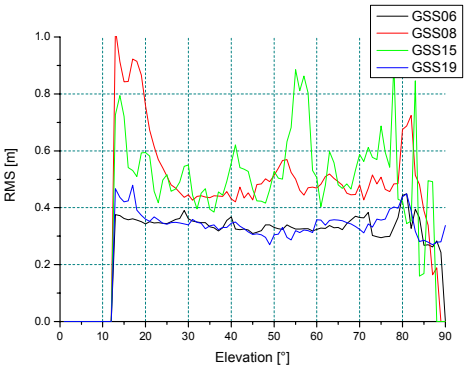

Figure 29: Range Accuracy after Synchronization (RMS), selected Stations

	Mean [m]	StdDev [m]	RMS [m]
Subset #1	-0.013	0.399	0.399
Subset #2	-0.014	0.396	0.397
Subset #3	-0.023	0.407	0.408
Subset #4	-0.036	0.413	0.414

Table 5: Range Accuracy After Synchronisation

As can be seen in figure 29 the range accuracy after synchronisation can be very different for each station. It is important to note, that the overall statistic of the different sensor station subsets (figure 28) is not affected significantly by removing one or two stations. All subsets show the same elevation independent performance of ca. 0.4 m.

SISE estimation performance

The results presented here are all obtained with the 3-parameter estimation algorithm at satellite level, which is the baseline for Galileo. In figure 31 the estimation error based on one week of real data is depicted for all satellites flagged as OK. The true SISE is obtained from IGS reference. As can be seen in the figure the main part of the distribution is on the right hand side of 0.0 m, and therefore the true SISE is likely to be over estimated.

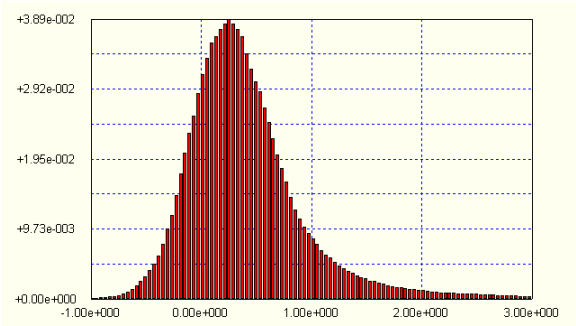

Figure 30: Estimation Error for satellites flagged as use [m]

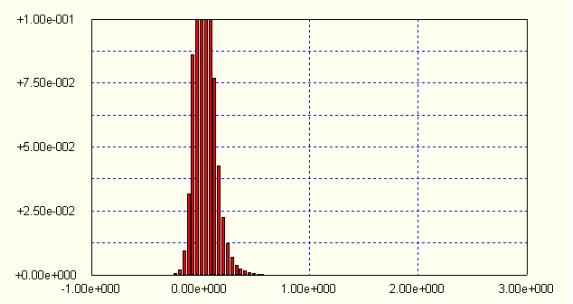

Figure 31: Estimation Error (noise = 0.1 m)

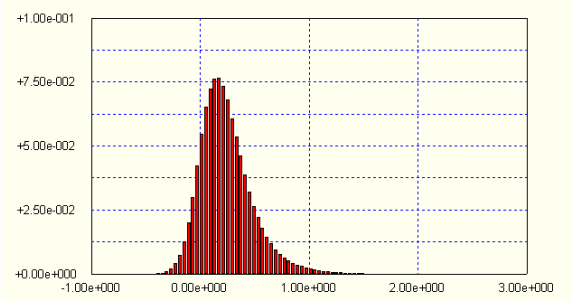

Figure 32: Estimation Error (noise = 0.3 m)

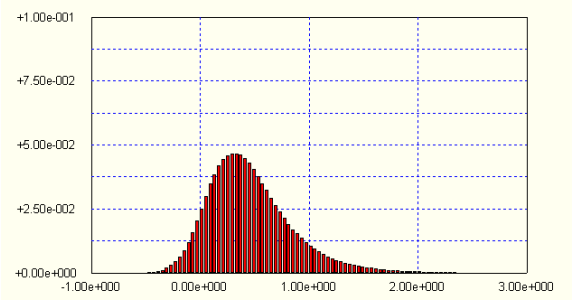

Figure 33: Estimation Error (noise = 0.5 m)

On one hand side this over estimation is linked to the definition of the SISE as absolute value and on the other hand it is linked to the noise level of the measurements after the pre-processing.

To quantify the impact of the noise level after the pre-processing some simulations have been performed. The sensor station network is identical to the real data processing to keep comparability as close as possible.

In figure 31 to 33 the impact of the noise level after the pre-processing is depicted. The noise level was simulated with a Gauss-Markov model and a correlation time of 600 seconds, which is linked to the filter time constant of the Hatch filter in the pre-processing.

From these figures is obvious that the over estimation increases with the noise level. The histogram with a noise level of 0.1 m is thinner and the peak is concentrated close to 0.0 m, whereas the histogram for 0.5 m noise is wider and the peak is shifted to the right.

By comparing the results of the real data (figure 30) with the simulated data (figure 32 and 33) it is visible, that these results fit quite well. By real data processing a range accuracy of ca. 0.4 m was obtained (see results of the pre-processing) and therefore the histogram should be between the noise level of 0.3 m and 0.5 m. The offset of the peak to the right side is 0.16 m for 0.3 m noise, 0.25 m for real data and 0.31 m for 0.5 m noise. The peak of the histogram for real data is lower than expected and the distribution is also wider. This is also an indicator for in-homogeneity of the network.

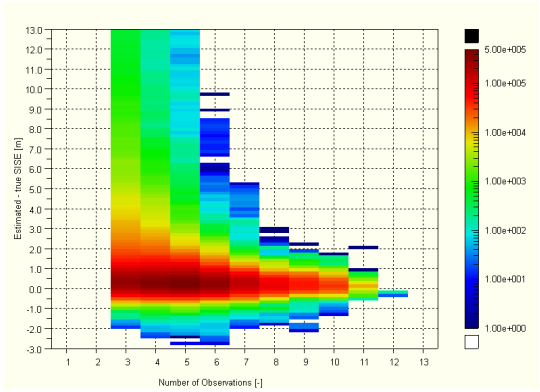

Figure 34: Estimation Error versus Number of observations for satellites flagged as use

The histogram in figure 30 shows a tail, which corresponds to a large estimation error. This tail is linked to the number of observations available for the SISE estimation. In figure 34 the estimation error is depicted versus the number of observations. The tail of the histogram is clearly linked to satellites observed by less than five or six observations.

SISMA bounding capability

For the Galileo integrity concept the SISMA was introduced to provide an indicator for the SISE estimation error. The performance of the SISMA, and thus of the SISE estimation, is evaluated by the probability that the standard deviation of the SISE estimation error exceeds the SISMA for all satellites flagged as USE. Galileo aims to provide a SISMA below 0.7 m for normal and 1.3 m for degraded modes of operation to the user. The results presented here regarding the SISMA are all based on real GPS measurements, and therefore not directly comparable with Galileo expectations. The main drivers for the SISMA computations are the quality of the measurements and the sensor station network. The inhomogeneous network of GSTB-V1 is not optimal with respect to Galileo expectations. Nevertheless the results are considered as representative under the environmental conditions of GPS.

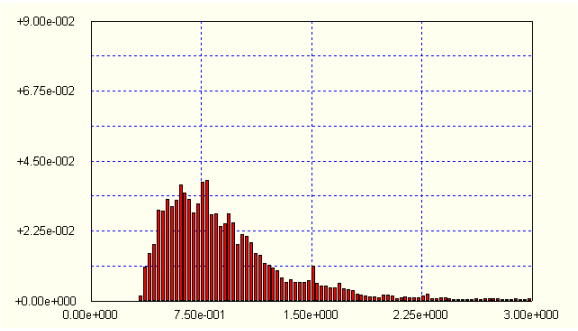

Figure 35: Distribution of SISMA for all satellite flagged as use

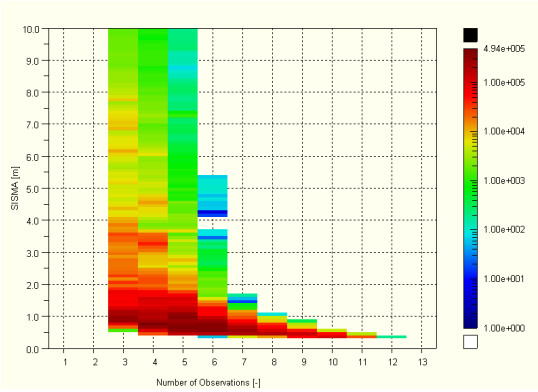

Figure 36: Distribution of SISMA for all satellite flagged as use versus Elevation

In figure 35 the distribution of the SISMA for the GSTB-V1 sensor station network with 25 stations is given. The UERE budget used for the SISMA computation was set to 0.5 m one sigma, which corresponds to the obtained overall pre-processing performance after synchronisation of 0.4 m with some margin.

The distribution of the SISMA shows a similar tail as the estimation error in figure 30. Form figure 36 it is obvious that this tail is also linked to low number of observations. As a consequence of this results there are three options to improve the SISMA. The first one is to extent the existing GSTB-V1 network to come up with a network close to DOC-6, which was done in the last months. The second possibility is to improve the quality of the input data, which is also limited due to the re-use of existing receivers. The improvement of the input data would lead to a lower UERE budget for the SISMA computation. The third option is to improve the chain of the pre-processing by further tuning of the algorithms.

Regarding this last option a new algorithm for synchronisation was developed for Galileo. This algorithm estimates the sensor station clocks based on common view technique. The preliminary results of this algorithm promises significant improvement for the range accuracy after the pre-processing.

Figure 37 shows the dependency between the SISE estimation error and the instantaneous SISMA. According to the definition of the SISMA, to be an indicator for the SISE estimation error, it is expected that for optimal conditions (no noise etc.) the SISMA is a measure of the estimation error. The red lines in the figure indicate the optimal SISMA.

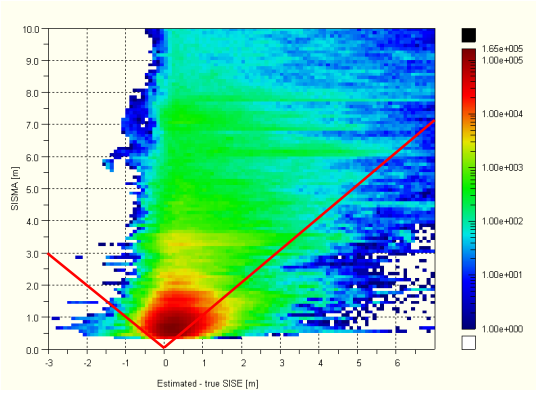

Figure 37: Estimation error versus SISMA fixed UERE budget

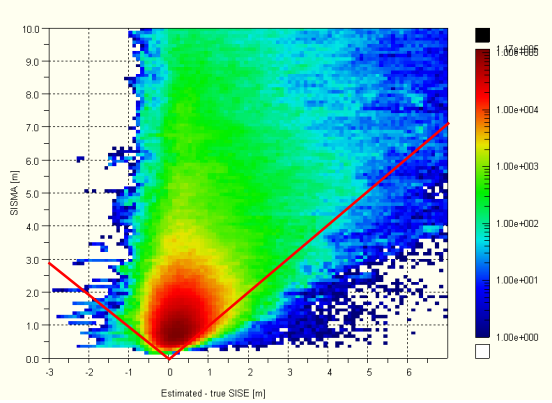

Figure 38: Estimation error versus SISMA variable UERE budget

As the performance of the SISMA is evaluated based on the standard deviation of the SISE estimation error the main samples should be close to the red lines for optimal conditions. The minimal SISMA achieved with a fixed UERE budget of 0.5 m for the given network is ca.0.25 m. The concentration of the samples above the red lines indicates that the fixed UERE budget is not always a conservative assumption.
In figure 38 the UERE budget for the SISMA computation was based on the standard deviation of the residuals used for the sensor station clock estimation. This standard deviation is a quasi real time indicator of the UERE budget to all LOS of one station. Therefore it takes the quality of the measurements to the stations into account and, thus, the impact of in-homogeneity of the network is reduced. The results are based on the same raw data and can be directly compared. The minimal SISMA achieved here is ca. 0.15 m, which is significant below the one of the fixed UERE budget. In addition it is visible that more of the samples are distributed 'better' between the red lines indicating a better match of the SISMA. The green area below the red lines in figure 38 is smaller as the green area in figure 37. For the area between –1 m and 1 m of the estimation error the shape of the samples (red dots) fits better to the optimal SISMA in the case of the variable UERE (figure 38) than for the fixed UERE (figure 37). In figure 37 a small white triangle is visible between the smallest SISMA and the red lines, this means the SISMA value is not able to follow the estimation error. This small triangle is not visible in figure 38 any more.
Nevertheless this variable UERE budget approach is still conservative and needs to be improved by algorithms to monitor the quality of the input data.

CONCLUSIONS AND WAY FORWARD

First commissioning phase results show that the complete integrity monitoring is indeed a direct function of the combined satellite and sensor station constellation. For this reason a good sensor station coverage of the southern hemisphere is necessary to provide the integrity service also in this part of the world.
In addition, the initial results show that using Galileo OD&TS and integrity algorithms the GPS constellation can already provide quite a good level of integrity.
All these results have been very promising, but of course the validity of the results depends on the validity of the assumptions. The results of the pre-processing and SISMA experiments show that the assumptions are quite valid. As, furthermore, similar assumptions have been used in all three analysed end-to-end scenarios (and two of them have been working on real-data), no nasty surprises should to be expected when the final Galileo system is considered.
Currently, the real data processing is based on real GPS measurements only. It is foreseen to upgrade the E-IPF to Galileo-like signal structures and the Galileo IOV (initial operational validation) scenario within a further stage of the project.
The Galileo integrity concept consolidation is ongoing mainly in terms of how SISA and SISMA values can be integrated at user level. Furthermore, the ground segment integrity monitoring algorithms definition is also ongoing in the current stage of the Galileo project. Modifications of the algorithms and new integrity barriers are anticipated to account for the individual ground sensor station characteristics.
Hence, further improvements in integrity system end-to-end performances are expected.

ACKNOWLEDGEMENTS

The GSTB-V1 project is funded by the European Space Agency as an experimentation platform to mitigate algorithm-related development risks. This paper expresses the personal opinion of the authors and does not reflect official opinions of ESA or IfEN.

REFERENCES

ESA (2003). *Galileo Reference Troposphere Model for the User Receiver*, European Space Agency, ESTEC, Noordwijk, June 30, 2003.

RTCA (1999). *Minimum Operational Performance Standards For Global Positioning System/Wide Area Augmentation System Airborne Equipment*, RTCA Document No.: RTCA/DO-229B, Prepared by RTCA Special Committee 159 (RTCA SC-159), RTCA, Inc., Washington, D.C., October 6, 1999.

Stanford University (1999). *http://waas.stanford.edu/metrics.html*.

Werner, W.; Deuster, I.; Amarillo-Fernandez, F. (2004). *Integrity Testcase Experimentation Results within GSTB-V1,* The European Navigation Conference GNSS 2004, Rotterdam, Netherlands, May 16-19, 2004

Werner, W.; Lemke, N.; Deuster, I.; Rossbach, U. (2003). *Integrity Investigations Within the European Galileo System Test Bed (GSTB),* Proceedings of the 16th International Technical Meeting of the Satellite Division of The Institute of Navigation, ION-GPS/GNSS 2003, Portland, Oregon, Sept. 9-12, 2003, pp. 2478-2486.